Applied Catalysis B: Environmental 144 (2014) 702–712

Contents lists available at ScienceDirect

Applied Catalysis B: Environmental

journal homepage: www.elsevier.com/locate/apcatb

Synthesis and characterization of Ag/AgCl–activated carbon composites for enhanced visible light photocatalysis

Joanne Gamage McEvoy[a], Wenquan Cui[b], Zisheng Zhang[a,*]

[a] University of Ottawa, Department of Chemical and Biological Engineering, 161 Louis Pasteur Private, Ottawa, ON K1N 6N5, Canada
[b] College of Chemical Engineering, Hebei United University, Tangshan 063009, PR China

ARTICLE INFO

Article history:
Received 21 February 2013
Received in revised form 18 June 2013
Accepted 26 July 2013
Available online 7 August 2013

Keywords:
Plasmon photocatalyst
Ag/AgCl
Visible light photocatalysis
Activated carbon

ABSTRACT

An adsorptive photocatalyst composite based on Ag/AgCl and activated carbon was proposed and investigated. The prepared composite was synthesized using impregnation-precipitation-photoreduction, and characterized by X-ray diffraction, transmission and scanning electron microscopies, X-ray photoelectron spectroscopy, N_2 sorption, and ultraviolet–visible diffuse reflectance spectrophotometry. The photoactivity of the composite was studied for the degradation of methyl orange and phenol under visible light. A mechanism for synergistic adsorption and photocatalysis by Ag/AgCl–AC was proposed, where the silver acts as the electron/hole generator, and polarization of the photoinduced charges relative to AgCl facilitates electron–hole separation, while the AC works to concentrate the pollutant around the active sites.

© 2013 Elsevier B.V. All rights reserved.

1. Introduction

In recent years, strategies for overcoming the low photocatalytic efficiencies realized with traditional TiO_2 photocatalysts have been developed through the design and fabrication of "second generation" photocatalysts, which have a greater visible light response and are engineered to reduce the rate of electron–hole recombination during the photocatalytic process. Some approaches proposed are through impurity doping [1], metals deposition [2–4], or sensitization [5,6].

An interesting phenomenon which has been used to prepare high efficiency visible-light-active photocatalysts is the localized surface plasmon resonance (SPR) exhibited by nanoparticles (NPs) of noble metals. This causes unique optical properties arising from collective oscillation of conduction electrons upon interaction with electromagnetic radiation, and can result in an amplified absorption of visible light in photocatalysts depending on the size and morphology of the NPs [7]. Silver NPs exhibiting SPR incorporated on silver halide structures have been used as plasmonic photocatalysts with extended visible light absorption, where the nanosilver and silver halide can also act in concert to polarize the photoinduced charges, facilitating electron–hole separation. The silver halide can also generate oxidizing species, such as •Cl or •Br (for Ag/AgCl and Ag/AgBr, respectively) [8].

Another approach for improving the efficiency of photocatalytic processes is through the immobilization on or incorporation of porous media with the catalyst [9,10]. Composite materials based on silver/silver halide plasmonic photocatalysts and carbonaceous nanostructures (such as graphene oxides [11,12], and graphene sheets [13]) have been previously explored, and these materials were shown to exhibit enhanced visible-light-induced photoactivity. Activated carbon can also be used in photocatalyst composites, and is well-suited to practical applications for water treatment systems due to the following reasons [14]: (1) AC is able to adsorb a wide range of organic compounds as well as natural organic matter, (2) it is widely available in many particle sizes at competitive costs, (3) its use and application in water and wastewater treatment are well-established compared to other support materials, and (4) AC-containing composites facilitate the ease of separation of nanosized photocatalysts from solution.

A synergistic increase in the photocatalytic activity of TiO_2 - AC composites has been observed [10], and can be attributed to the presence of a common contact interface between solids, whereby the pollutants can be adsorbed by AC, and migrate continuously to the supported photocatalyst [15]. The AC support may also affect the dynamics of photo-induced charges [16]. However, the need for incorporation of visible-light-active photocatalysts into AC composites has been emphasized in literature [14].

In this work, enhanced visible-light-active Ag/AgCl–AC composite photocatalysts are proposed and synthesized, and their activity is investigated for the degradation of methyl orange dye (MO) and phenol organic pollutants. The composites prepared combine the enhanced visible light absorption and photocatalytic efficiency

* Corresponding author. Tel.: +1 613 562 5800x6110; fax: +1 613 562 5172.
E-mail addresses: jgamage@uottawa.ca (J. Gamage McEvoy), wkcui@163.com (W. Cui), zzhang@uottawa.ca (Z. Zhang).

0926-3373/$ – see front matter © 2013 Elsevier B.V. All rights reserved.
http://dx.doi.org/10.1016/j.apcatb.2013.07.062

gained using silver/silver halide plasmonic photocatalysts with the synergy of adsorption obtained through incorporation within the AC matrix to create hybrid composites.

2. Experimental

2.1. Synthesis of Ag/AgCl–AC composites

Ag/AgCl–AC composites were prepared using an impregnation-precipitation-photoreduction method. Typically, 1 g of unmodified Darco G60 activated carbon (100 mesh, Sigma–Aldrich) was impregnated in 20 mL of aqueous $AgNO_3$ (ACS grade, MP Biomedicals Inc.) of a certain concentration. The mixture was sonicated for 10 min, and then stirred magnetically for 6 h. 20 mL of HCl (reagent-grade, Fisher Scientific) was then added in a 50% stoichiometric excess under magnetic stirring for 2 h to induce the precipitation of deposited $AgNO_3$ into AgCl. The reduction of some AgCl was then carried out via irradiation by a 300 W UV–vis light source (Ushio ELH) for 1 h. The mixture was then filtered and dried in air overnight. The prepared Ag/AgCl–AC composite powders were gently ground before use. The prepared samples are denoted by weight ratio of Ag to AC (Ag:AC), calculated as if all of the AgCl was reduced to Ag. Reference Ag/AgCl was prepared using the same synthesis procedure omitting the AC impregnation step, and AgCl was prepared similarly without photoreduction.

2.2. Characterization

X-ray diffraction (XRD) patterns of all prepared powders were collected using a Rigaku Ultima IV XRD with a Cu K(α) source (λ = 0.15418 nm) operating at 40 kV and 44 mA. Transmission electron microscopy imaging was performed using a FEI (formerly Phillips) Tecnai F20 G2 field emission transmission electron microscope (TEM) at an acceleration voltage of 200 keV. The samples were dispersed in water and dropped onto a copper grid for observation. The morphology of the samples (coated in Au/Pd alloy using an Anatech Hummer VII sputter coater) was studied using a Tescan VegaII XMU field emission scanning electron microscope (SEM). The chemical states of the photocatalysts were analyzed by XSAM800 X-ray photoelectron spectroscopy (XPS), and the patterns were deconvoluted using XPSPEAK41 software. The surface areas, total pore volumes, and microporosity data were obtained from N_2 adsorption–desorption isotherms collected at 77 K using an automatic adsorption apparatus (Nova 4200E, Quantachrome). The samples were outgassed at 50 °C under N_2 flow for 1 h at a pressure of 760–770 mm Hg. The Brunauer, Emmett, and Teller (BET) surface areas were calculated using the adsorption isotherms in the range of $P/Po < 0.015$. The total pore volumes were calculated using the volumes of adsorbed N_2 at $P/Po = 0.975$, and the t-plot method was used to calculate micropore volumes and external surface areas. Ultraviolet–visible (UV–vis) diffuse reflectance spectra were measured using a UV–vis spectrophotometer (Puxi, UV 1901) equipped with an integrating sphere attachment and on a Thermo Evolution 300 spectrophotometer equipped with a Praying Mantis diffuse reflectance accessory over the range of 230–800 nm.

2.3. Photocatalytic degradation experiments

2.3.1. Photoreactor

To quantify the photocatalytic degradation of organic pollutants using the composite powders, a slurry reactor was set up in a reflective housing to prevent outside light from entering the system. Illumination was provided by a 300 W ELH tungsten halogen bulb (Ushio) with a UV filter (Kenko Zeta, $\lambda > 410$ nm, transmittance > 90%) at a distance of 10 cm from the beaker. The irradiation was measured using a quantum meter (Biospherical QSL-2100; 400 nm < λ < 700 nm), and was found to be approximately 4.7×10^{-3} Einstein m^{-2} s^{-1}. Cooling was provided by an external cooling jacket, and the temperature of the reaction was controlled to 20 °C ± 2.

2.3.2. MO adsorption and photodegradation

For the combined adsorption–photocatalysis tests, 0.5 g L^{-1} catalyst was added to a 200 mL solution containing reagent-grade MO (Fisher Scientific) and immediately exposed to illumination under constant magnetic stirring at 180 rpm for 2 h. The adsorption-only tests were performed using the same procedure in the absence of light. For the prolonged photocatalysis tests, 200 mL of MO solution was allowed to equilibriate in the dark with 0.5 g L^{-1} catalyst under constant magnetic stirring at 180 rpm for 2 h prior to each experiment. The photocatalytic degradation was then allowed to proceed for 2.5 h in the presence of visible light irradiation. For all tests, samples were drawn periodically and centrifuged, and the supernatant analyzed using a spectrophometer (Genesys 10UV, ThermoScientific). The peak absorbance used for MO was λ = 463 nm for pH > 4 and λ = 505 for pH < 3. The initial MO concentration was kept at 25 mg L^{-1} except for in the concentration studies. The initial pH of the solution was left unadjusted at pH 5.5, except for in the pH studies. For the pH studies, the initial pH was adjusted with either 0.5 M HCl or 0.5 M NaOH (reagent-grade, Fisher Scientific). The pH was measured with a benchtop pH probe (accumet AB15+ Basic, Fisher Scientific). Recyclability tests were performed by centrifuging the reaction medium between runs at 3500 rpm for 3 min in a Hermle Z400K centrifuge (Hermle Labortechnik GmbH), removing the supernatant, and redispersing the catalyst in fresh MO solution. The quenching experiments were performed by the addition of appropriate radical scavengers. 0.01 M isopropanol (reagent-grade, Fisher Scientific) was used as the radicals scavenger, 0.01 M ethylenediaminetetraacetate disodium salt dihydrate (EDTA) (99%, Sigma–Aldrich) was used as the holes scavenger, and N_2 bubbling was used to suppress the formation of superoxide radicals, respectively. The removal efficiency was calculated using the following formula:

$$\text{Removal efficiency } (\%) = \frac{C_o - C_t}{C_o} \times 100 \quad (1)$$

where C_o denotes the initial pollutant concentration (mg L^{-1}), and C_t is the concentration at time t (mg L^{-1}). For prolonged runs including a dark adsorption time, C_o was taken as the adsorption equilibrium concentration. Control runs were performed in the absence of light and catalyst, respectively. The error associated to the experiments was estimated as the standard deviation between triplicate runs.

2.3.3. Phenol adsorption and photodegradation

Adsorption and photodegradation of phenol (98%, Fisher Chemical) was also studied using the same methodology and parameters as in the MO experiments, but the initial concentration used was 13 mg L^{-1}, and the supernatant was analyzed at a peak absorbance of λ = 270 nm.

3. Results and discussion

3.1. Catalyst characterization

The phase structure and crystallinity of the prepared samples were investigated by XRD, and the obtained spectra for the composites and for pure AC and Ag/AgCl are shown in Fig. 1, respectively. The AC exhibited mainly amorphous structure, with the exception of a wide, shallow hexagonal (0 0 2) graphitic peak, which indicated small regions of crystallinity as in other commercial activated carbons [17]. The prepared composites exhibited similar spectra and

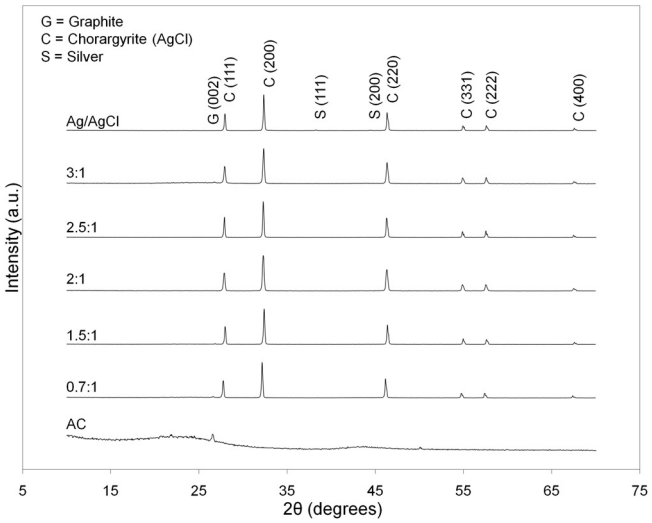

Fig. 1. XRD spectra for AC, Ag/AgCl, and various Ag/AgCl–AC composites.

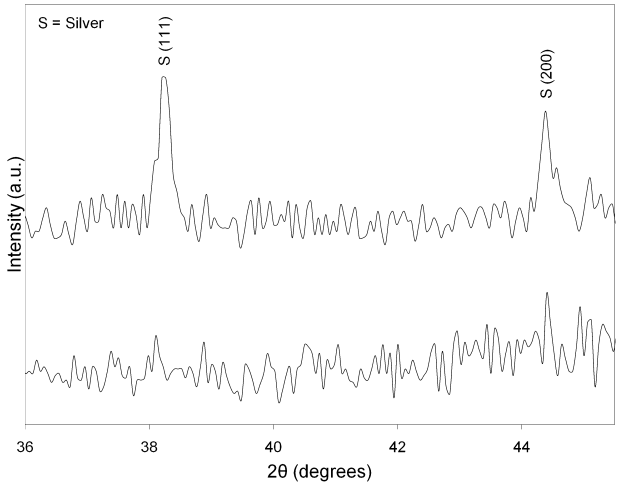

Fig. 2. XRD spectra for Ag/AgCl, and 2.5:1 Ag/AgCl–AC composite.

crystallinity to the pure Ag/AgCl, as indicated by the peak positions and intensities. The diffraction peaks were indexed to face centred cubic AgCl phase (JCPDS card # 31-1238) with lattice constants of $a = 5.545–5.549$ Å, in good agreement with the literature value for AgCl ($a = 5.549$ Å [18]). From the enlarged spectra shown in Fig. 2, the main diffraction peaks for the (1 1 1) plane at 38.1° and for the (2 0 0) plane at 44.3° for metallic Ag (JCPDS card #01-087-0597) were observed for the pure Ag/AgCl material, implying that the *in situ* reduction was able to promote the transformation of some AgCl to Ag. However, the peaks associated to metallic silver could not be observed in the spectra for a representative Ag/AgCl–AC composite (2.5:1), which may have been due to its low content, small particle size, and high dispersion on the surface of AgCl – AC, as was reported for Ag/AgI – Al_2O_3 prepared using deposition-precipitation-photoreduction synthesis [19].

The structure of the composites was studied by TEM, and images of a representative Ag/AgCl–AC (2.5:1), and the as-prepared Ag/AgCl are shown in Fig. 3. For pure Ag/AgCl, the AgCl particles were found to range from approximately 1.7 to 2.1 μm, and were decorated with smaller metallic silver clusters in the order of 120–160 nm on their exterior. The high-resolution TEM of the silver clusters formed indicated an interlayer *d*-spacing of 0.24 nm, which corresponded to the Ag (1 1 1) plane of silver. The selected area diffraction pattern (SAED) shown in the inset of Fig. 3b indicated that the sample was polycrystalline in nature, and the rings were attributed to diffraction from the (1 1 1), (2 0 0), and (2 2 0) reflections of fcc silver (JCPDS card #01-087-0597), based on the calculated *d*-spacings of 2.47 Å, 2.12 Å, and 1.45 Å, respectively. For the Ag/AgCl–AC composite, the TEM images indicated that deposition of the photocatalyst occurred mainly on the exterior surface of the activated carbon (which was identifiable by the large, light, grainy structure in Figs. 3c and 3d), and the darker, more electron-dense regions attributable to silver/silver halides formed heterogeneous clusters on its outer surface.

To further investigate the morphology of the Ag/AgCl–AC, SEM imaging was performed, and the results are presented in Fig. 4. The deposition of Ag/AgCl was found to form clusters resulting in high coverage of the AC, although some exposed surfaces of the textured carbon host material were observable. Metallic silver was also found on the surface of the silver halides, although it was not easily observed in the TEM due to the thickness and three dimensional nature of the Ag/AgCl clusters formed on the face of the composite. The AgCl particles in Ag/AgCl–AC were found by SEM to range from 470 nm to 1.06 μm, and the reduced Ag were approximately 110–150 nm. The photochemical reduction *in situ* has been reported to generate Ag atoms which aggregate to form silver nanograins that deposit on the surface of AgCl particles [13], in good agreement with the results obtained in this study.

The surface chemical states of the samples were investigated by XPS. Spectra from the high-resolution scans of Cl 2p and Ag 3d orbits are given for a representative Ag/AgCl–AC composite (2.5:1) and for as-prepared Ag/AgCl in Fig. 5a and b, respectively. The deconvoluted peaks for the Cl 2p orbits were centred at approximately 197.6 eV and 199.2 eV for both Ag/AgCl and the prepared composite. These peaks corresponded well to Cl 2p 3/2 and Cl 2p 1/2, indicating the presence of chlorine as Cl^- [20,21]. The silver peaks at approximately 366.8 eV and 372.8 eV were ascribed to the binding energies of Ag 3d 5/2 and Ag 3d 3/2, respectively, for Ag^+ present in AgCl [20,22]. The smaller peaks obtained at 367.7 eV and 373.8 were assigned to the binding energies of Ag 3d 5/2 and Ag 3d 3/2, respectively, for metallic Ag [23]. This indicated that the silver was present as Ag^+ in AgCl and as Ag^0 in metallic Ag, further evidencing the photoreduction of some AgCl to Ag under UV–vis irradiation.

The BET surface areas calculated by N_2 adsorption are summarized in Table 1, and were found to vary between 63.0 and 279.3 m^2/g for the composites. The BET range used was $P/Po < 0.015$, based on a criteria proposed by Rouquérol et al. [24] for materials possessing microporosity. The composite surface areas were also expressed relative to activated carbon, and were found to consistently decrease with increasing Ag/AgCl content. This was thought to be due to the effects of pore-blocking by the Ag/AgCl particles. The surface areas of all of the composites were smaller than that of activated carbon, but were all larger than that of pure Ag/AgCl, indicative of an increased adsorptive capability of the AC composites compared to the bare photocatalyst alone.

The structure and porosity of the composites were studied, and the nitrogen adsorption–desorption isotherm for a representative

Table 1
Characteristics of prepared composites.

Catalyst	BET surface area (m^2/g)	Relative surface area (%)
AC	810.9	100
0.7:1 composite	279.3	34
1.5:1 composite	149.2	18
2:1 composite	105.5	13
2.5:1 composite	77.1	9.5
3:1 composite	63.0	7.8
Ag/AgCl	2.1	2.6

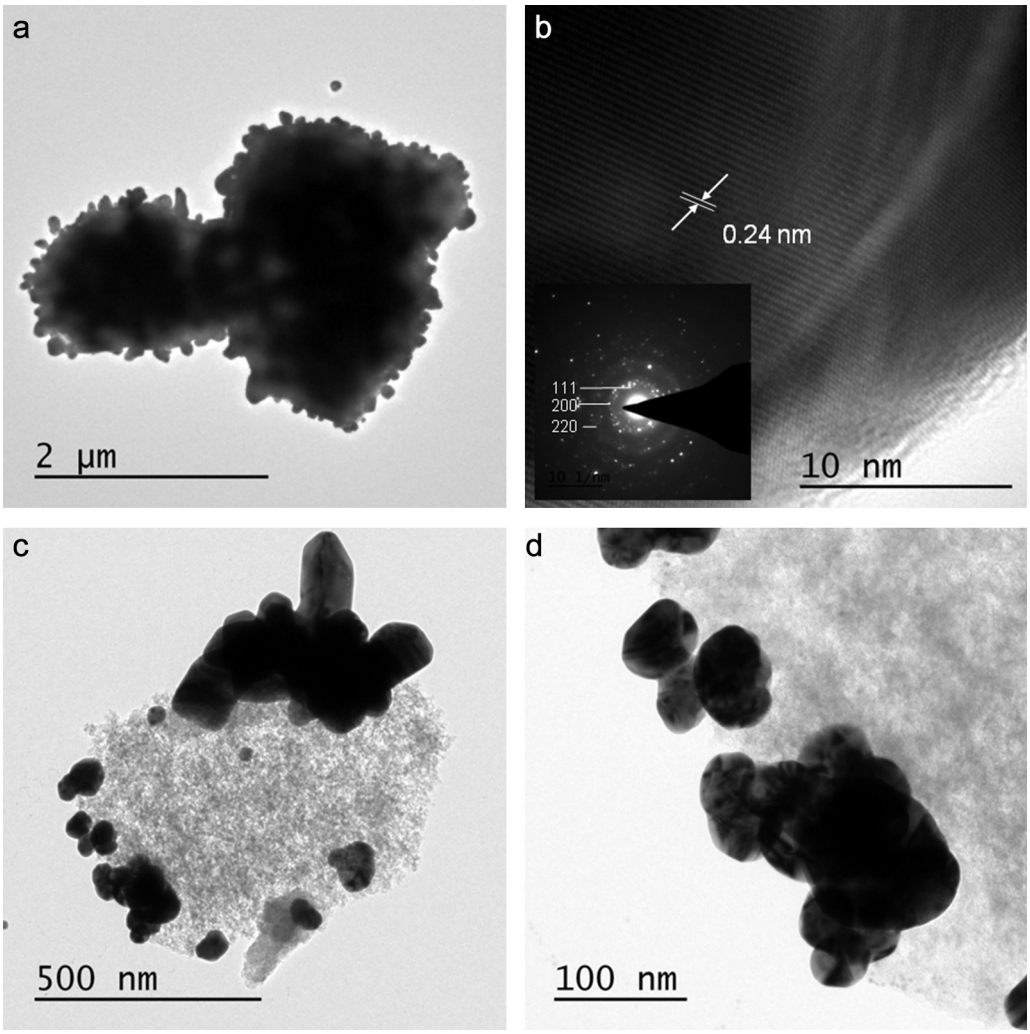

Fig. 3. TEM images of (a) Ag/AgCl; (b) high-resolution TEM of Ag in Ag/AgCl; SAED pattern inset; and (c and d) as-prepared Ag/AgCl–AC composite (2.5:1).

sample (2.5:1) is given in Fig. 6, with that of AC shown for comparison. The isotherms observed for both the composite and for pure AC were Type IV according to the IUPAC classification [25], and the H4 hysteresis in the desorption branch was due to the presence of mesopores [26].

The total pore volumes, microporosity and mesoporosity data are summarized in Table 2. The total pore volume, as well as the micro- and mesopore volumes (and consequently, areas) all decreased significantly upon addition of Ag/AgCl into the composites. The constructed *t*-plots indicated that microporosity significantly contributed to the total pore volume. For AC, the micropores contributed 44% of the total pore volume, while this was decreased to approximately 36% in the composite. Based on observations of the composite and the sizes of Ag/AgCl observed, the photocatalyst did not penetrate the micropores of AC (<2 nm), but formed an "egg-shell" structure, where clusters of photocatalyst were deposited on the outer surface of AC [27]. These clusters decreased the pore volume and surface area by blocking the mesopores and pore entrances present on the AC surface. This pore blockage would have also caused a reduction in micropore volume, since the mesopores in AC were the main throughfares to the micropores for sorption [27]. Based on the trend in BET surface areas, increasing the Ag/AgCl content in the composites was thought to enhance this pore blocking effect.

The UV–vis absorption data for a representative Ag/AgCl–AC composite (2.5:1), as-prepared Ag/AgCl, and unreduced AgCl are given in Fig. 7, respectively. For all the samples, an absorbance edge at ~385 nm was observed due to the band gap absorption of AgCl ($E_{bg,indirect}$ = 3.25 eV [28]). Compared to the unreduced AgCl, the prepared Ag/AgCl catalyst showed a broad absorption band in the range of 400–800 nm, which was thought to be attributable to the surface plasmon resonance of Ag NPs produced during photoreduction. The broadness of the peak was caused by multiple plasmonic oscillation frequencies present because of variation in the shapes

Table 2
Porosity characteristics.

Catalyst	Total pore volume (cm^3/g)	Micropore volume (cm^3/g)	Micropore area (m^2/g)	Mesopore volume[a] (cm^3/g)	Mesopore area (m^2/g)
AC	0.61	0.27	510	0.34	201
2.5:1	0.070	0.025	48.0	0.045	26.1

[a] Calculated by difference.

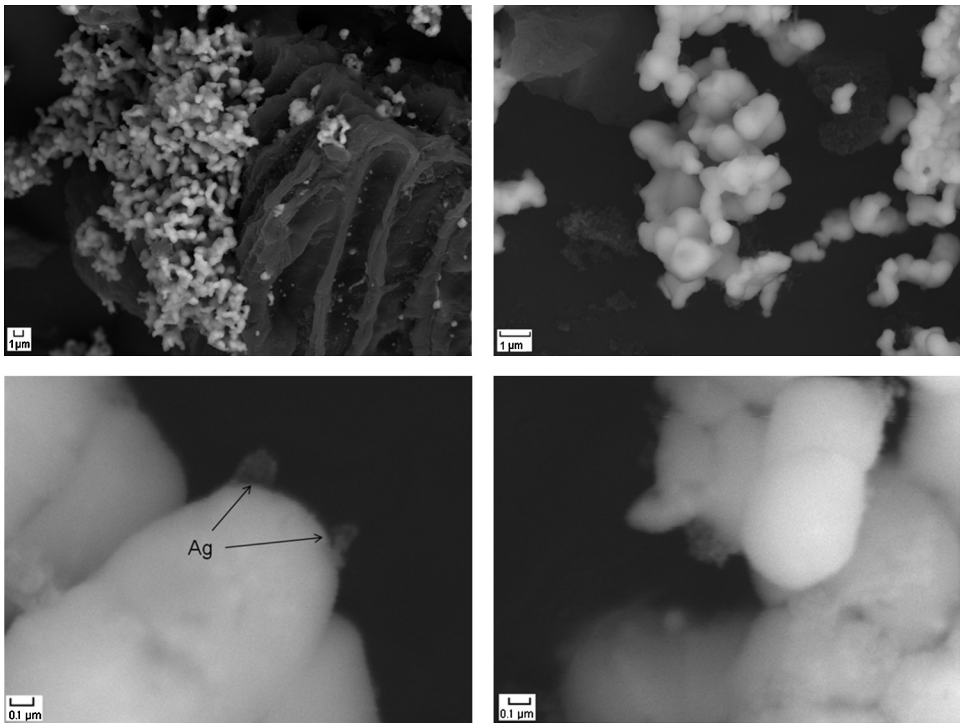

Fig. 4. SEM images of prepared Ag/AgCl–AC composite (2.5:1).

and diameters of Ag NPs formed [7,29,30]. The Ag/AgCl–AC composite also showed broad, strong absorbance in the visible light region, which indicated that it possessed good applicability as a visible-light-active photocatalyst.

3.2. Photocatalytic activity

3.2.1. MO adsorption and photodegradation

Preliminary screening for activity of the prepared composites was performed using a combined adsorption–photocatalysis process to compare the final MO removal observed to that obtained using dark adsorption only [31,32]. The results from the rapid screening tests are given in Fig. 8. Preliminary trials using pure Ag/AgCl indicated negligible removal under dark adsorption conditions, and 15.1% MO removal under visible light irradiation, while the unmodified AC was able to completely adsorb MO from solution in under 10 min. Additionally, total MO removal in the absence of catalyst was found to be less than 1.5%, and the effects of photolysis were therefore thought to be negligible.

The MO removal efficiencies were calculated and are given in Table 3. The Ag/AgCl–AC composites exhibited much higher adsorptive capabilities than pure Ag/AgCl, and this was thought to be due to their larger surface areas. The prepared composites also had very high adsorptive capabilities compared to other Ag/AgX – carbon composites reported in literature such as Ag/AgCl – reduced graphene oxide sheets [13]. A noticeable enhancement in removal efficiency between the dark adsorption and combined adsorption–photocatalysis was realized for the composites containing a high loading of Ag/AgCl (2:1, 2.5:1, and 3:1 ratios). This increased efficiency under irradiation was thought to be attributable to the production of photoexcited species by the photocatalytic component of the composites. The increase not proportional to the additive effects of adsorption and photocatalysis, since the efficiency observed for a full loading (0.5 g L^{-1}) of Ag/AgCl was 15.1%, and the composites contained the photocatalyst in lower amounts (a nominal dosage of 0.5 g composite per L was used). This suggested the presence of a synergistic effect of adsorption on the photocatalytic removal efficiency, as reported for other adsorbent photocatalysts such as TiO_2 on AC [33]. Although there may have been radical generation at the lower Ag/AgCl compositions (0.7:1, 1.5:1), the enhancement under irradiation was not realized using the present conditions due to the almost full removal of MO by adsorption only.

Table 3
MO removal efficiencies obtained in various processes.

Catalyst	Final removal efficiency: $(C_o - C_f)/C_o$ (%)
Pure Ag/AgCl (adsorption only)	Negligible
Pure Ag/AgCl (adsorption + photocatalysis)	15.1
0.7:1 (adsorption only)	98.6
0.7:1 (adsorption + photocatalysis)	98.1
1.5:1 (adsorption only)	98.0
1.5:1 (adsorption + photocatalysis)	97.9
2:1 (adsorption only)	91.7
2:1 (adsorption + photocatalysis)	97.3
2.5:1 (adsorption only)	73.8
2.5:1 (adsorption + photocatalysis)	88.1
3:1 (adsorption only)	55.1
3:1 (adsorption + photocatalysis)	77.6

To further investigate photocatalysis mediated by the composite catalysts, prolonged runs were carried out using a 2 h dark adsorption time, followed by visible light irradiation. The results obtained are shown in Fig. 9, as amount of MO removed from solution per weight of catalyst used (or equivalent dose, in the case of AC).

It has been proposed in literature that the presence of irradiation can result in an increase of adsorption of pollutants onto AC in TiO_2-AC composites, as studied for methylene blue dye under UV irradiation [34]. To investigate this in the current system, a control experiment was performed using AC only, at an equivalent proportion as that incorporated into the 2.5:1 composite. From the results shown in Fig. 9, the irradiation provided did not induce

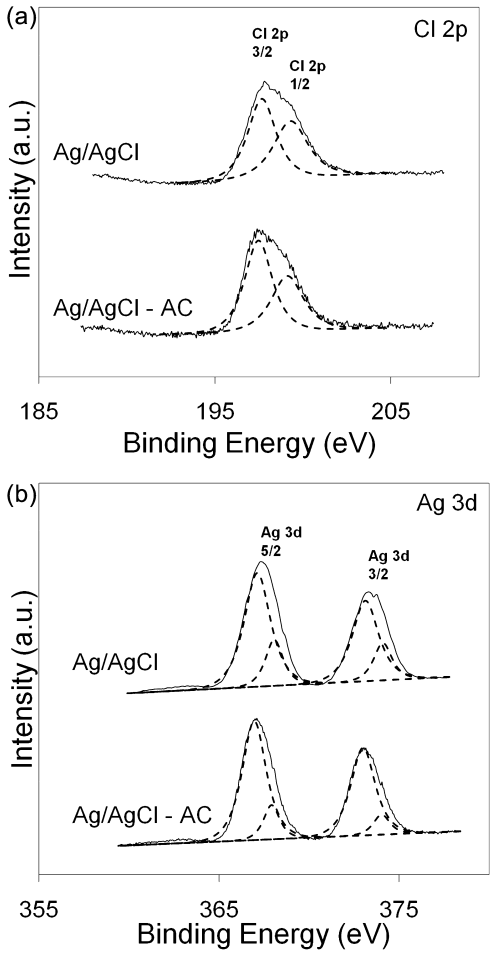

Fig. 5. (a) Cl 2p XPS spectra for as-prepared Ag/AgCl and 2.5:1 Ag/AgCl–AC composite (b) Ag 3d XPS spectra for as-prepared Ag/AgCl and 2.5:1 Ag/AgCl–AC composite.

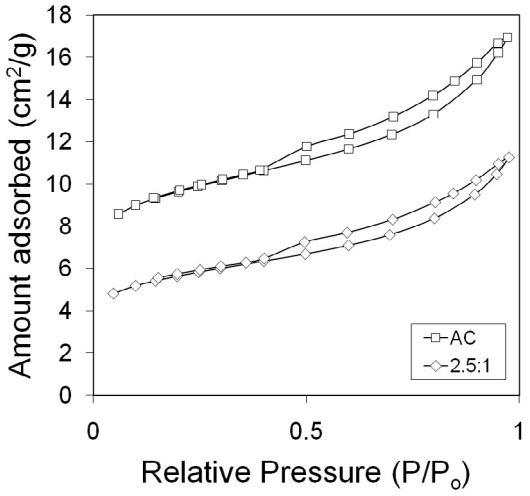

Fig. 6. N_2 adsorption–desorption isotherms for AC and 2.5:1 Ag/AgCl–AC composite.

a significant change in the adsorption of dye onto activated carbon. In contrast, the composite catalysts exhibited a noticeable increase in the removal rate of MO upon illumination, after the pseudo-equilibrium was reached. This was thought to be due to the visible light absorption and consequent photocatalytic effect in the composites, removing the MO pollutant by photodegradation. These results also suggested that the prepared Ag/AgCl–AC

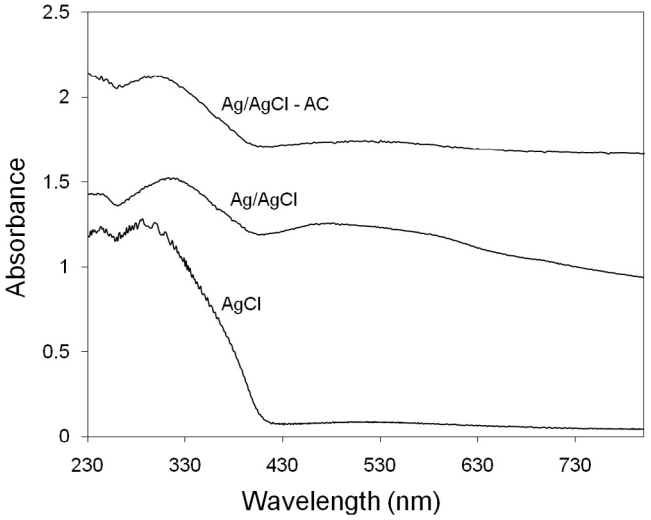

Fig. 7. UV–vis absorption spectra of 2.5:1 Ag/AgCl–AC composite, as-prepared Ag/AgCl, and unreduced AgCl, respectively.

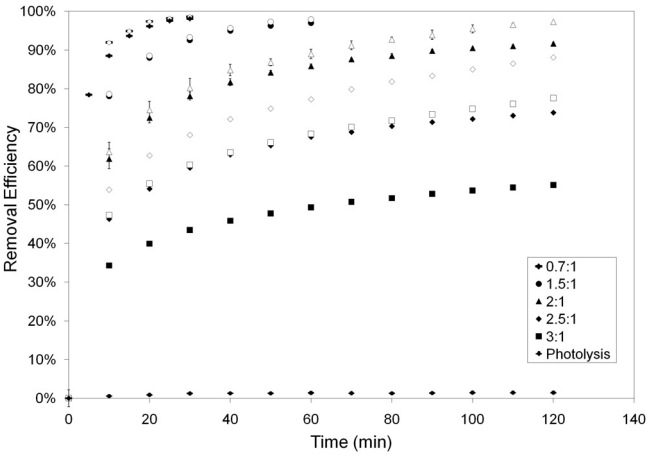

Fig. 8. Comparison of adsorption and combined adsorption–photocatalysis for Ag/AgCl–AC composite powders (where the darkened markers represent adsorption and their open counterparts, photocatalysis-adsorption; respectively) – average of three trials, representative error bars shown.

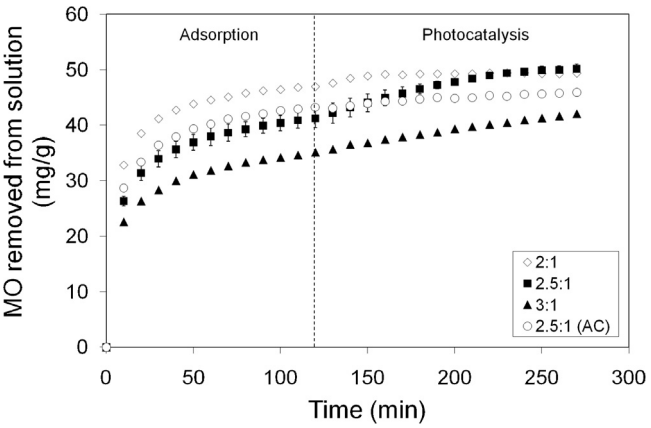

Fig. 9. Adsorption and subsequent photocatalysis using 2:1, 2.5:1, and 3:1 Ag/AgCl–AC, respectively. The prolonged test using an equivalent loading of AC as that incorporated into the 2.5:1 composite is shown for comparison – representative error bars shown.

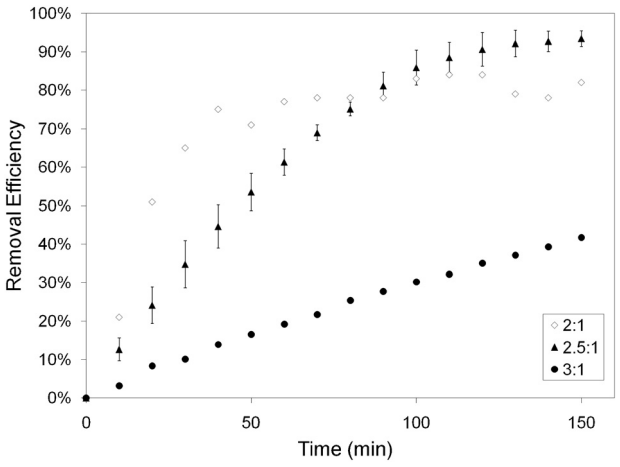

Fig. 10. Photocatalytic removal efficiency as a function of time for 2:1, 2.5:1, and 3:1 Ag/AgCl–AC composites, respectively – representative error bars shown.

samples were able to remove MO from solution by a dynamic adsorption–photocatalysis mechanism under visible light.

The data from the prolonged adsorption–photocatalysis studies shown in Fig. 9 were normalized using the concentrations at the end of dark adsorption as the initial concentrations for photocatalytic reaction, and the calculated temporal removal efficiencies for photocatalysis are given in Fig. 10. The Langmuir–Hinshelwood kinetic expression for heterogeneous surface reactions was used to describe the data, where the reaction rate is described by the following expression.

$$-\frac{dC}{dt} = K\frac{kC}{1+KC} \tag{2a}$$

where K is the Langmuir Hinshelwood adsorption coefficient ($L\,mg^{-1}$), and k is the reaction rate constant ($mg\,L^{-1}\,min^{-1}$). Simplification of this kinetic expression into a pseudo first order equation is frequently employed in cases where the initial concentration used is sufficiently small ($<10^{-3}$ mol L^{-1} [35]). The simplified, integrated rate expression is given by:

$$\ln\left(\frac{C_o}{C}\right) = k't \tag{2b}$$

where k' denotes the pseudo first order rate constant (min^{-1}). This apparent rate constant has been cited to be appropriate for the comparison of different photocatalytic systems, since it is independent of concentration and enables the calculation of photocatalytic activity independently of dark adsorption [36]. To compare the rates obtained using various composites, the rate constants were calculated by Eq. (2b) for the initial linear portion of the reaction, and the fitted data is shown in comparison with the experimental values in Fig. 11.

The initial rate constants obtained from the slope of the fitted lines for the 2:1, 2.5:1, and 3:1 composites were 0.0345, 0.0128, and 0.0037 min^{-1}, respectively, and was 0.0032 min^{-1} for an Ag/AgCl prolonged run control. The regression coefficient (R^2) associated to the fitted data ranged from 0.948 to 0.997, and the fit was thought to be appropriate to model the initial stages of degradation. The synergy factor (R) for activated carbon composite photocatalysts, defined by Matos et al. [10] and adapted in this case for a pure Ag/AgCl reference catalyst, was calculated by equation 3:

$$R = \frac{k'(\text{Ag/AgCl–AC})}{k'(\text{Ag/AgCl})} \tag{3}$$

where R was essentially a ratio of the pseudo first order kinetic constants. This yielded synergy factors of 10.8, 4, and 1.2 for the 2:1, 2.5:1, and 3:1 composites, respectively. The synergy factor for

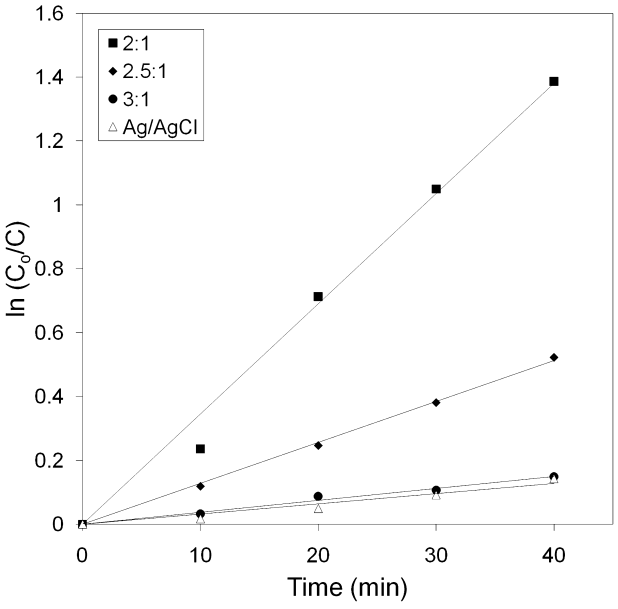

Fig. 11. Photocatalytic degradation reaction kinetics for 2:1, 2.5:1, and 3:1 Ag/AgCl–AC composites and Ag/AgCl, respectively.

the 3:1 composite was near unity because the loss of adsorptive capability caused by excessive Ag/AgCl loading led to a decrease in removal rate severe enough to make its activity comparable to that obtained using a full (i.e. 0.5 g L^{-1}) loading of pure Ag/AgCl alone. However, for the lower loaded composites, the synergy factors were much greater than 1, indicating the presence of AC enhanced the overall removal efficiency.

The removal behaviour upon irradiation was thought to be strongly influenced by the adsorptive capability of the composites, where the powder with high surface area (i.e. 2:1), exhibited a fast removal rate due to its high adsorptive capability, and vice versa for the low surface area composite (3:1). While an increased MO removal rate from solution did not necessarily mean all of the pollutant was being degraded photocatalytically, the adsorptive capability of the catalyst was presumed to promote the transfer of pollutants from solution to the reactive sites. It should be noted that increasing the Ag/AgCl ratio in the composite may have provided a greater number of reaction sites, but also decreased the total adsorption by reducing the surface area, so a tradeoff was required between the desired adsorptive and photocatalytic capabilities of the composites. As a temporary optimum, the 2.5:1 powder was chosen for further study to illustrate the dynamic adsorptive-photocatalytic behaviour of the designed catalysts.

3.2.2. *Effect of initial MO concentration*

The effect of initial MO concentration on the activity was investigated in the range of 25–50 ppm, and the results are shown in Fig. 12. While all of the prolonged runs performed exhibited some photodegradation using the composite catalyst, the activity tended to decrease with increasing MO concentration. The lowest final degradation (13.2%) was realized using an initial concentration of 50 ppm, while the highest final degradation (93.8%) was achieved at 25 ppm. The observed difference may have been due to the effect of pollutant concentration on the light penetration into solution [37]. The solution transmittance decreased with increasing concentration, resulting in fewer photons reaching the catalyst surface, and a consequent reduction in degradation activity. This result was consistent with literature for the effect of initial MO concentration on photocatalysis [37–40]. To investigate whether the increased light penetration at lower initial concentrations affected MO photolysis,

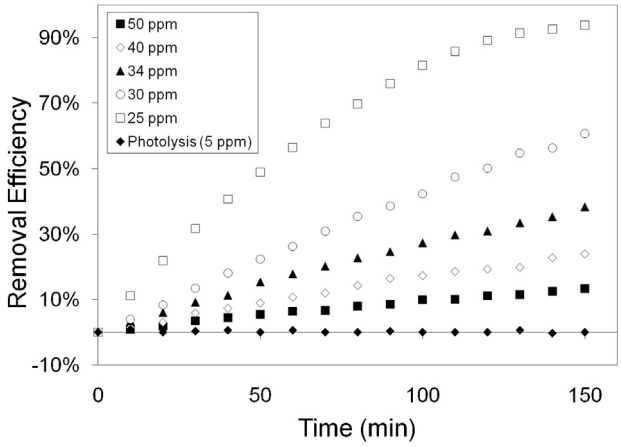

Fig. 12. Effect of initial concentration on photodegradation using 2.5:1 composite.

the photolytic conversion at an initial concentration of 5 ppm was measured, and was found to remain negligible, as shown in Fig. 12.

3.2.3. *Effect of pH*

The solution pH has been reported to be a very important parameter in photocatalytic processes [35,41,42]. The pH can affect the catalyst–pollutant interactions and the generation of redox species during irradiation [39,43]. The initial solution pH was investigated between the range of pH 2–9.5 by adjusting with HCl or NaOH. The results obtained from the degradation are shown in Fig. 13. It should be noted that the photolysis did not change significantly between acidic and basic media, and was thought to have a negligible contribution to the change in degradation observed.

From the data obtained, the pH was found to strongly affect the photocatalytic process, with degradation taking place more rapidly in acidic solution, and decreasing with increasing pH.

This may have been due to the change of surface charge properties with changes in pH for methyl orange and the consequent change in adsorption affinity towards the catalyst. MO existed in its anionic state in water at pH 7 and above due to the sodium ion dissociation. In acidic conditions, amphoteric MO was formed because hydrogen became attached to nitrogen in the azo bond associated with the ring structure [44]. The two MO structures are shown schematically in Fig. 14.

The surface of AgCl particles has been asserted in literature to be likely terminated by Cl^- ions [45], and was therefore

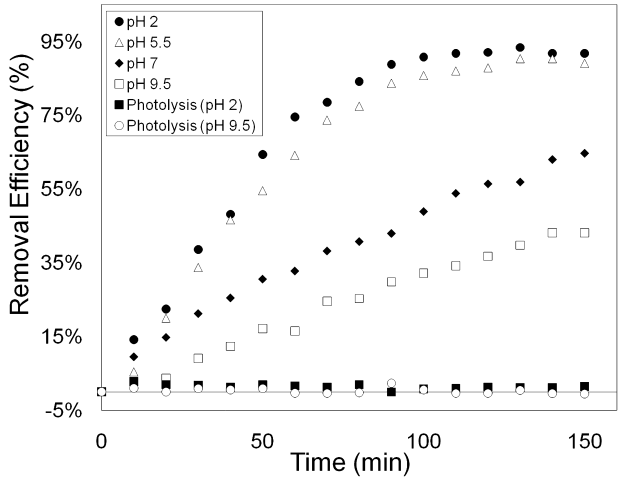

Fig. 13. Effect of pH on photodegradation using 2.5:1 composite.

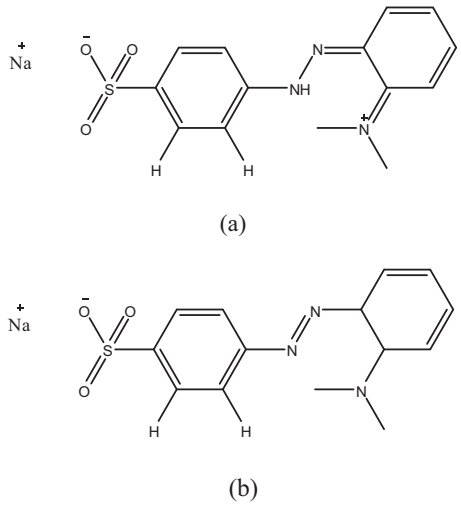

Fig. 14. Methyl orange structure in acidic and basic media: (a) and (b), respectively.

negatively charged. Additionally, the polarization of electron distribution within the metallic Ag on the surface would lead to regions of its negative and positive charges being far from and close to the Ag/AgCl interface, respectively [45]. Therefore, the surface of the Ag/AgCl was likely negatively charged. The interaction of these negatively charged catalyst surfaces with anionic MO in alkaline solution may have caused Coloumbic repulsion, resulting in a decreased amount of substrate adsorbed. This effect was not present in acidic media, where MO took on an amphoteric structure. The photocatalytic activity of anionic (mainly sulphonated) dyes was found in other literature to reach a maximum in acidic conditions, and decreased in the pH range of 7–11 [46], which is in good agreement with the results obtained in this study.

It should be noted also that while electrostatic attractions and repulsions between the pollutant and catalyst affected activity, the interpretation of data at variable pH is difficult in practice due to the different redox species present. At low pH values, positive holes are considered the major oxidation species, while at neutral or high pH, hydroxyl radicals are the predominant species present [42,43,47–50]. The elucidation of degradation mechanism therefore becomes difficult, since the dye could be degraded through hydroxyl radical attack, directly oxidized by a positive hole, or directly reduced by a negative electron in the conduction band. These factors also influenced the activity results observed at various pH levels.

3.2.4. *Recyclability*

To evaluate the recyclability of the composite catalysts prepared, the 2.5:1 sample was used in four consecutive trials, recovering the catalyst in between runs by centrifuging and decanting. The MO removal by adsorption and degradation in the sequential runs is shown in Fig. 15, respectively.

The adsorption of MO using the composite catalyst was found to decrease between consecutive runs. This was due to the limited adsorption capacity of the recycled composite, and the inability of the photocatalyst portion to fully regenerate the AC by degrading all of the adsorbed MO. The latter effect also resulted in a decrease in photocatalytic activity with repeated use because the rate of degradation was low compared to the rate of accumulation of the substrate. This caused saturation at the surface of the photocatalyst, diminishing its photonic efficiency [51]. The gradual decrease in efficiency could be observed with repeated use, and in the second to fourth trials, the photocatalyst was able to degrade 75%, 67%, and 62% of the total MO degraded in the first run, respectively. The

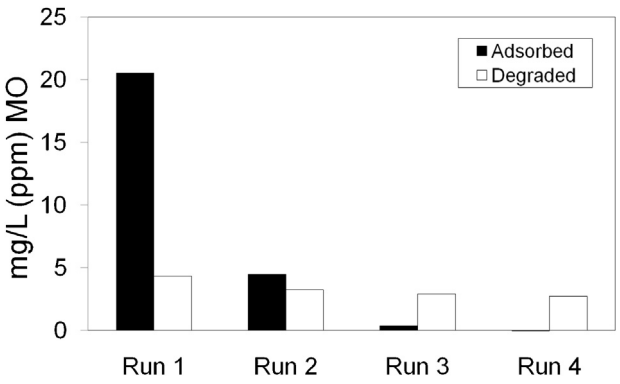

Fig. 15. Adsorption and degradation performance of 2.5:1 composite over four consecutive runs.

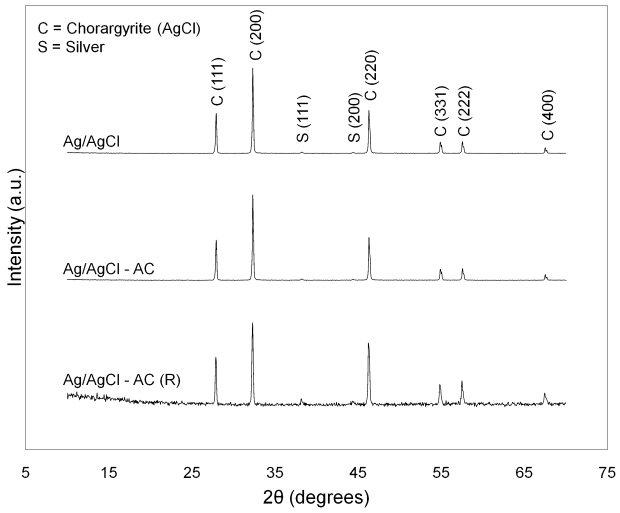

Fig. 16. XRD spectra for as-prepared Ag/AgCl, 2.5:1 Ag/AgCl–AC composite, and recycled 2.5:1 Ag/AgCl–AC composite after four adsorption–photocatalysis cycles.

decreased efficiency with increased cycle number may have also been due to the formation of reaction intermediates and their subsequent adsorption and accumulation on the photocatalyst surface [52,53], or limitations in diffusion of the pollutant from the inner pores of the composite to the actual catalytic sites [54].

The XRD pattern for the composite catalyst after use in four consecutive runs is shown in Fig. 16, with the fresh catalyst pattern for comparison. The spectra observed before and after recycling were nearly identical, indicating good stability of the catalyst. Small peaks at 38.1° and 44.3° attributable to the (1 1 1) and (2 0 0) faces of metallic silver, respectively, were observed in the used sample. The appearance of these peaks was thought to be due to an increase of Ag nanoparticle size during the visible-light-induced photocatalysis, caused by aggregation and photodecomposition of some AgCl to form metallic Ag clusters. However, this decomposition has been found to have only a small effect on the total surface contents of Ag and AgCl, as per previous reports using similar experimental conditions [21,45,55], confirming the overall stability of such catalysts in repeated use.

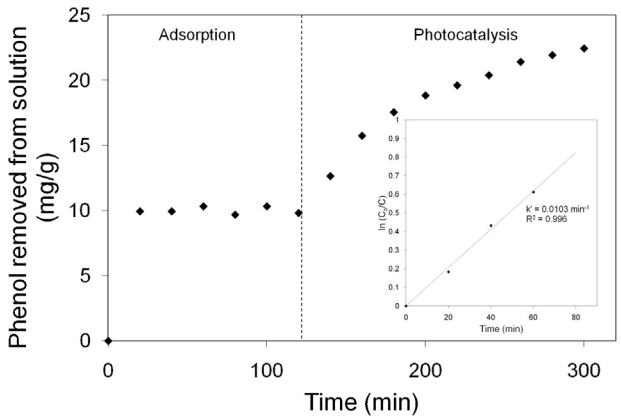

Fig. 17. Adsorption and subsequent photocatalysis using 2.5:1 Ag/AgCl–AC in 13 mg L^{-1} phenol solution. Photocatalytic degradation kinetics are shown inset.

3.2.5. Role of photo-induced species

Radical and hole trapping experiments were designed to investigate the roles of the photo-induced h^+ and e^- in the prepared composites through the use of appropriate quenchers. The quenching effect of scavengers can be employed as a diagnostic tool to discern the relative importance of various photo-induced species present [56], where the rate of photocatalytic reaction may be partly suppressed by the employed quencher, resulting in a lowered apparent rate constant (k'). The magnitude of this reaction suppression is indicative of the relative role the species plays in the reaction. Nitrogen bubbling was used to reduce the dissolved oxygen in solution, limiting the capture of photo-induced electrons by molecular oxygen to generate superoxide radicals. EDTA was used as a hole scavenger, while isopropanol was used as a hydroxyl radical scavenger. The EDTA itself had a negligible effect on the adsorption capacity of AC, as previously reported [57]. The kinetic data obtained using various suppressants is given in Table 4.

From the observed change in kinetics, it was found that the hydroxyl radical did not play a dominant role in the photocatalytic oxidation due to its weak quenching effect, consistent with other studies on Ag/AgX-type catalysts [20,56,58]. The holes were found to have a more pronounced effect, as indicated by the observed decrease in reaction rate upon addition of EDTA. Holes were thought to act by two pathways, namely through direct surface reaction with the dye, or by oxidation of chloride ions in AgCl to form chlorine radicals, which subsequently oxidized the dye. The superoxide radical formed by molecular oxygen was also found to play a significant role in the photocatalytic oxidation. The predominance of these two species in photocatalytic dye degradation using an Ag/AgCl – modified catalyst was also found by Xiong et al. [58].

3.2.6. Activity for phenol degradation

The photocatalytic activity for degradation of a colorless organic compound, phenol, was investigated to confirm a surface plasmon resonance-induced photocatalytic process took place using the Ag/AgCl–AC composite, and not merely a photosensitization of the organic MO dye under visible light irradiation [59]. The results from the adsorption and subsequent photocatalysis, as well as the calculated degradation kinetics, are shown in Fig. 17. The composite exhibited high activity for phenol degradation, converting

Table 4
Kinetic data in the presence of various scavengers for 2.5:1 composite.

	Species suppressed	k' ($\times 10^{-2}$ min^{-1})	R^2	k'/k' (no quenching) (%)
N_2 bubbling	Superoxide radical ($^{\bullet}O_2^-$)	0.28	0.99	21.9
Isopropanol	Hydroxyl radical ($^{\bullet}OH$)	0.11	0.99	85.9
EDTA	Positive charge vacancy (hole, h^+)	0.31	0.96	24.2

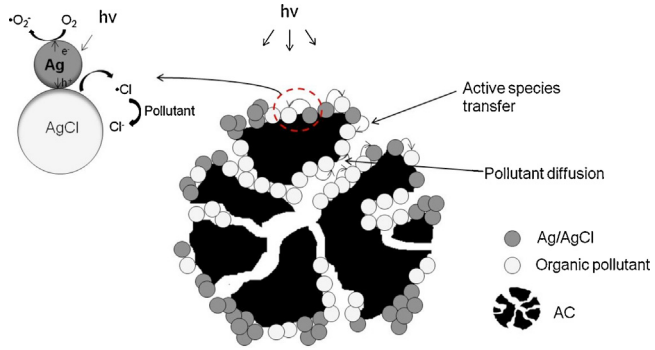

Fig. 18. Mechanism of Ag/AgCl–AC photocatalysis on an organic pollutant. Adapted from [64].

approximately 13 mg phenol per gram composite under illumination, while the photolytic conversion was found to be negligible. The photocatalysis-induced transformation was greater than the phenol adsorption observed in the dark, and the pseudo first order rate constant calculated using Eq. (2b) was found to be 0.0103 min^{-1}. The phenol photodegradation results confirmed the visible light photoactivity of the Ag/AgCl composite.

3.2.7. *Mechanism of action*

The mechanism of photocatalytic action of the composites is thought to be related to the localized surface plasmon resonance of the silver nanoparticles deposited on the Ag/AgCl structures. In this system, a visible light photon can be absorbed by a silver nanoparticle, generating a hole and an electron. These can be effectively polarized by the surface plasmon resonance state of the silver, causing efficient separation of the hole and electron such that the electron is transferred to the silver surface furthest away from the interface with AgCl, and the hole transferred to the AgCl particle surface [45]. The stability of silver on silver halides has been attributed to this charge separation, which prevents the generated electron from being transferred to the Ag^+ ions in AgCl [60]. The electron is instead transferred to molecular oxygen, which is present at the surface, forming active species such as the superoxide anion of oxygen, which can facilitate degradation of the organic pollutant (MO or phenol) [61]. The positive hole generated can oxidize the Cl^- ions into •Cl, which are powerful oxidizing agents that can attack organic pollutants near the surface of the catalyst [40], reducing the •Cl atoms back to their ionic state.

The activated carbon in the composites provides adsorption sites for the pollutant. The adsorbed pollutant can then migrate to the Ag/AgCl decomposition centers located on the AC surface, due to the concentration gradients present [62]. In the absence of a highly adsorbent AC support, the pollutant must collide with the photocatalyst and maintain efficient contact for the reaction to occur. If this contact is not maintained, the reactants or intermediates will desorb back into solution. The AC also plays a role in allowing chain photocatalytic reactions to proceed more easily by the retention of intermediate products on its surface. Additionally, the AC surface has many more adsorption sites than the neat Ag/AgCl, which reduces the likelihood of pollutant molecules colliding with the catalyst but not being adsorbed due to surface area limitations [63]. The process is shown schematically in Fig. 18.

4. Conclusions

In this work, novel composite photocatalysts based on Ag/AgCl and activated carbon were synthesized by an impregnation-precipitation-reduction method. The prepared composites were found to have an "egg-shell" structure, although some pore-blocking of AC occurred due to the incorporated Ag/AgCl. The composites had good photocatalytic activity for MO and phenol degradation under visible light. The role of the radical species was elucidated through quenching experiments, and the holes and oxygen radicals were found to be dominant for photodegradation. Some decrease in activity was observed with cyclic use, so future work on this catalyst should include investigations in improving its recyclability, such as through prolonged light exposure to regenerate the activated carbon surface [62]. The effect of the activated carbon in the composite should also be studied, and parameters such as particle size, porosity, and pretreatment investigated in relation to their effect on the structural and morphological characteristics of the synthesized Ag/AgCl–AC. For example, it has been proposed that a smaller particle size can facilitate AC regeneration, since the desorbed pollutants could have shorter diffusion paths to the active sites on the exterior surface of the catalyst [14]. The effect of light intensity on the composite should also be explored, and the material tested under real sun conditions to validate its applicability to solar systems, such as for use in solar AC regeneration schemes [65]. Due to the high adsorption capability observed, the adsorption characteristics of the composite should be described according to appropriate mechanistic considerations.

Acknowledgements

This work was supported by The Natural Sciences and Engineering Research Council of Canada and the National Natural Science Foundation of China (Grant No. 50972037 and 51172063). The authors would like to acknowledge the Centre for Catalysis Research and Innovation and the Department of Earth Sciences (University of Ottawa), Qi Yueli and colleagues at the College of Chemical Engineering (Hebei United University), and Dr. Jiangqun Wang (Carleton University) for help with sample characterization.

References

[1] W.Y. Choi, A. Termin, M.R. Hoffmann, Journal of Physical Chemistry 98 (1994) 13669–13679.
[2] G. Zhao, H. Kozuka, T. Yoko, Thin Solid Films 277 (1996) 147–154.
[3] C.M. Wang, A. Heller, H. Gerischer, Journal of the American Chemical Society 114 (1992) 5230–5234.
[4] I.M. Arabatzis, T. Stergiopoulos, M.C. Bernard, D. Labou, S.G. Neophytides, P. Falaras, Applied Catalysis B 42 (2003) 187–201.
[5] R.W. Fessenden, P.V. Kamat, Journal of Physical Chemistry 99 (1995) 12902–12906.
[6] J.M. Stipkala, F.N. Castellano, T.A. Heimer, C.A. Kelly, K.J.T. Livi, G.J. Meyer, Chemistry of Materials 99 (1997) 2341–2353.
[7] P. Wang, B. Huang, X. Zhang, X. Qin, H. Jin, Y. Dai, Z. Wang, J. Wei, J. Zhan, S. Wang, J. Wan, M.-H. Whangbo, Chemistry: A European Journal 15 (2009) 1821–1824.
[8] A. Pourahmad, S. Sohrabnezhad, E. Kashefian, Spectrochimica Acta A 77 (2010) 1108–1114.
[9] H. Slimen, A. Houas, J.P. Nogier, Journal of Photochemistry and Photobiology A 221 (2011) 13–21.
[10] J. Matos, J. Laine, J.M. Hermann, Applied Catalysis B 18 (1998) 281–291.
[11] M. Zhu, P. Chen, M. Liu, Journal of Materials Chemistry 21 (2011) 16413–16419.
[12] M. Zhu, P. Chen, M. Liu, ACS Nano 5 (2011) 4529–4536.
[13] H. Zhang, X. Fan, X. Quan, S. Chen, H. Yu, Environmental Science and Technology 45 (2011) 5731–5736.
[14] T.-T. Lim, P.-S. Yap, M. Srinivasan, A.G. Fane, Critical Reviews in Environmental Science and Technology 41 (2011) 1173–1230.
[15] X. Wang, Y. Liu, Z. Hu, Y. Chen, W. Liu, G. Zhao, Journal of Hazardous Materials 169 (2009) 1061–1067.
[16] S. Basha, D. Keane, A. Morrissey, K. Nolan, M. Oelgemöller, J. Tobin, Industrial and Engineering Chemistry Research 49 (2009) 11302–11309.
[17] W. Li, C. Liang, W. Zhou, J. Qiu, Z. Zhou, G. Sun, Q. Xin, Journal of Physical Chemistry B 107 (2003) 6292–6299.
[18] D. Chen, S.H. Yoo, Q. Huang, G. Ali, S.O. Cho, Chemistry: A European Journal 18 (2012) 5192–5200.
[19] C. Hu, T. Peng, X. Hu, Y. Nie, X. Zhou, J. Qu, H. He, Journal of the American Chemical Society 132 (2010) 857–862.
[20] J. Jiang, L. Zhang, Chemistry: A European Journal 17 (2011) 3710–3717.
[21] P. Wang, B. Huang, Z. Lou, X. Zhang, X. Qin, Y. Dai, Z. Zheng, X. Wang, Chemistry: A European Journal 16 (2010) 538–544.
[22] M. Zayat, D. Einot, R. Reisfeld, Journal of Sol-Gel Science and Technology 10 (1997) 203–211.

[23] P. Gangopaghyay, R. Kesavamoorthy, S. Bera, P. Magudapathy, K.G.M. Nair, B.K. Panigrahi, S.V. Narasimnhan, Physical Review Letters 94 (2005), 047403(1)–047403(4).
[24] J. Rouquérol, P. Llewellyn, F. Rouquérol, Studies in Surface Science and Catalysis 160 (2007) 49–56.
[25] K.S.W. Sing, D.H. Everett, R.A.W. Haul, L. Moscou, R.A. Pierotti, J. Rouquérol, T. Siemieniewska, Pure and Applied Chemistry 57 (1985) 603–619.
[26] J. Rouquérol, D. Avnir, C.W. Fairbridge, D.H. Everett, J.H. Haynes, N. Pernicone, J.D.F. Ramsay, K.S.W. Sing, K.K. Unger, Pure and Applied Chemistry 66 (1994) 1739–1758.
[27] X. Zhang, L. Lei, Journal of Hazardous Materials 153 (2008) 827–833.
[28] S. Glaus, G. Calzaferri, Photochemical & Photobiological Sciences 2 (2003) 398–401.
[29] P. Jain, W. Huang, M. El-Sayed, Nano Letters 7 (2007) 2080–2088.
[30] J.-F. Guo, B. Ma, A. Yin, K. Fan, W.-L. Dai, Journal of Hazardous Materials 211/212 (2012) 77–82.
[31] R. Jiang, H.-Y. Zhu, G.-M. Zeng, L. Xiao, Y.-J. Guan, Journal of Central South University of Technology 17 (2010) 1223–1229.
[32] Y. Tang, Z. Jiang, Q. Tay, J. Deng, Y. Lai, D. Gong, Z. Dong, Z. Chen, RSC Advances 2 (2012) 9406–9414.
[33] J. Matos, J. Laine, J.-M. Hermann, D. Uzcategui, J.L. Brito, Applied Catalysis B 70 (2007) 461–469.
[34] A.Y. Khan, D.W. Mazyck, Carbon 44 (2006) 182–184.
[35] J.-M. Hermann, Catalysis Today 53 (1999) 115–129.
[36] J. Matos, J. Laine, J.-M. Herrmann, Journal of Catalysis 200 (2001) 10–20.
[37] F. Akbal, Environmental Progress 24 (2005) 317–322.
[38] V. Nam, J. Kim, G. Han, Chemosphere 47 (2002) 1019–1024.
[39] N. Guettai, H. Ait Amar, Desalination 185 (2005) 427–437.
[40] D. Wang, Y. Duan, Q. Luo, X. Li, L. Bao, Desalination 270 (2011) 174–180.
[41] Y. Wang, Water Research 34 (2000) 990–994.
[42] H. Lachheb, E. Puzenat, A. Houas, M. Ksibi, E. Elaloui, C. Guillard, J.M. Hermann, Applied Catalysis B 39 (2002) 75–90.
[43] W.Z. Tang, Z. Zhang, H. An, M.O. Quintana, D.F. Torres, Environmental Technology 18 (1997) 1–12.
[44] E. Akama, A.J. Tong, M. Ito, S. Tanaka, Talanta 48 (1999) 1133–1137.
[45] P. Wang, B. Huang, X. Qin, X. Zhang, Y. Dai, J. Wei, M.-H. Whangbo, Angewandte Chemie International Edition 47 (2008) 7931–7933.
[46] I.K. Konstantinou, T.A. Albanis, Applied Catalysis B 49 (2004) 1–14.
[47] C. Guillard, H. Lachheb, A. Houas, M. Ksibi, E. Elaloui, J.M. Hermann, Journal of Photochemistry and Photobiology A 158 (2003) 27–36.
[48] I. Poulios, I. Tsachpinis, Journal of Chemical Technology and Biotechnology 74 (1999) 349–357.
[49] V. Augugliaro, C. Baiocchi, A.B. Prevot, E. García-López, V. Loddo, S. Malato, G. Marcí, L. Palmisano, M. Pazzi, E. Pramauro, Chemosphere 49 (2002) 1223–1230.
[50] G.A. Epling, C. Lin, Chemosphere 46 (2002) 561–570.
[51] J. Araña, J.L. Martínez Nieto, J.A. Herrera Melián, J.M. Doña Rodríguez, O. Gondález Díaz, J. Pérez Peñam, O. Bergasa, C. Alvarez, J. Méndez, Chemosphere 55 (2004) 893–904.
[52] S.X. Liu, X.Y. Chen, X. Chen, Journal of Hazardous Materials 143 (2007) 257–263.
[53] Y.H. Ao, J.J. Xu, D.G. Fu, X.W. Shen, C.W. Yuan, Colloids and Surfaces A 312 (2008) 125–130.
[54] C.-C. Mao, H.-S. Went, Environmental Progress & Sustainable Energy 31 (2011) 306–317.
[55] D. Wang, Y. Duan, Q. Luo, X. Li, J. An, L. Bao, L. Shi, Journal of Materials Chemistry 22 (2012) 4847–4854.
[56] G. Li, K.H. Wong, X. Zhang, C. Hu, J.C. Yu, R.C.Y. Chan, P.K. Wong, Chemosphere 76 (2009) 1185–1191.
[57] S. Mukherjee, S. Kumar, A.K. Misra, M. Fan, Chemical Engineering Journal (**129**, 2007) 133–142.
[58] W. Xiong, Q. Zhao, X. Li, D. Zhang, Catalysis Communications 16 (2011) 229–233.
[59] T. Wu, G. Liu, J. Zhao, H. Hidaka, N. Serpone, The Journal of Physical Chemistry B 102 (30) (1998) 5845–5851.
[60] H. Xu, H. Li, J. Xia, S. Yin, Z. Luo, L. Liu, L. Xu, ACS Applied Materials & Interfaces 3 (2011) 22–29.
[61] J. Yu, G. Dai, B. Huang, Journal of Physical Chemistry C 113 (2009) 16394–16401.
[62] W. Li, S. Liu, Adsorption 18 (2012) 67–74.
[63] R. Leary, A. Westwood, Carbon 49 (2011) 741–772.
[64] K.Y. Foo, B.H. Hameed, Advances in Colloid and Interface Science 159 (2010) 130–143.
[65] P.-S. Yap, T.-T. Lim, Water Research 46 (2012) 3054–3064.